

Functional Implication of β -Carotene Hydroxylases in Soybean Nodulation^{1[C][W][OA]}

Yun-Kyoung Kim², Sunghan Kim², Ji-Hyun Um, Kyunga Kim, Sun-Kang Choi, Byung-Hun Um, Suk-Woo Kang, Jee-Woong Kim, Shinichi Takaichi, Seok-Bo Song, Choon-Hwan Lee, Ho-Seung Kim, Ki Woo Kim, Kyoung Hee Nam, Suk-Ha Lee, Yul-Ho Kim, Hyang-Mi Park, Sun-Hwa Ha, Desh Pal S. Verma, and Choong-Il Cheon*

Department of Biological Science (Y.-K.K., S.K., J.-H.U., K.H.N. C.-I.C.) and Department of Statistics (K.K.), Sookmyung Women's University, Seoul 140-742, Korea; Gangneung Science Industry Foundation, Gangneung 210-340, Korea (S.-K.C.); Natural Products Research Center, KIST Gangneung Institute, Gangneung 210-340, Korea (B.-H.U., S.-W.K.); Electron Microscopy Laboratory, Dental Research Institute (J.-W.K.), and School of Plant Science (S.-H.L.), Seoul National University, Seoul 151-742, Korea; Department of Biology, Nippon Medical School, Nakahara, Kawasaki 113-8602, Japan (S.T.); Department of Functional Crops, National Institute of Crop Science, Milyang 441-857, Korea (S.-B.S.); Department of Molecular Biology, Pusan National University, Busan 609-735, Korea (C.-H.L., H.-S.K.); School of Ecological and Environmental Systems, Kyungpook National University, Sangju 702-701, Korea (K.W.K.); National Institute of Crop Science, Suwon 441-857, Korea (Y.-H.K., H.-M.P.); Graduate School of Biotechnology and Crop Biotech Institute, Kyung Hee University, Yongin 446-701, Korea (S.-H.H.); and Biotechnology Center, Ohio State University, Columbus, Ohio 43210 (D.P.S.V.)

Legume-*Rhizobium* spp. symbiosis requires signaling between the symbiotic partners and differential expression of plant genes during nodule development. Previously, we cloned a gene encoding a putative β -carotene hydroxylase (*GmBCH1*) from soybean (*Glycine max*) whose expression increased during nodulation with *Bradyrhizobium japonicum*. In this work, we extended our study to three *GmBCHs* to examine their possible role(s) in nodule development, as they were additionally identified as nodule specific, along with the completion of the soybean genome. In situ hybridization revealed the expression of three *GmBCHs* (*GmBCH1*, *GmBCH2*, and *GmBCH3*) in the infected cells of root nodules, and their enzymatic activities were confirmed by functional assays in *Escherichia coli*. Localization of *GmBCHs* by transfecting Arabidopsis (*Arabidopsis thaliana*) protoplasts with green fluorescent protein fusions and by electron microscopic immunogold detection in soybean nodules indicated that *GmBCH2* and *GmBCH3* were present in plastids, while *GmBCH1* appeared to be cytosolic. RNA interference of the *GmBCHs* severely impaired nitrogen fixation as well as nodule development. Surprisingly, we failed to detect zeaxanthin, a product of *GmBCH*, or any other carotenoids in nodules. Therefore, we examined the possibility that most of the carotenoids in nodules are converted or cleaved to other compounds. We detected the expression of some carotenoid cleavage dioxygenases (*GmCCDs*) in wild-type nodules and also a reduced amount of zeaxanthin in *GmCCD8*-expressing *E. coli*, suggesting cleavage of the carotenoid. In view of these findings, we propose that carotenoids such as zeaxanthin synthesized in root nodules are cleaved by *GmCCDs*, and we discuss the possible roles of the carotenoid cleavage products in nodulation.

Legume-*Rhizobium* spp. symbiosis results in the formation of the root nodule, in which rhizobia fix atmospheric nitrogen. Nodule development requires

diverse events, such as Nod factor synthesis in the rhizobia, perception of the Nod factor on plant roots by receptor-like kinases, endocytosis of rhizobia into plant cells, and so on (Stacey et al., 2006; Oldroyd et al., 2011; Singh and Parniske, 2012). Sequential expression of numerous plant genes occurs during nodulation, contributing to different stages including nitrogen fixation. Arbuscular mycorrhizal (AM) symbiosis exhibits many similarities to the nodulation process (Oldroyd et al., 2009). For example, *SymRK*, the receptor-like kinase gene, is required for both rhizobial and AM symbioses (Stracke et al., 2002). Similarly, the signal transduction pathways following perception are also in part the same, and the genes common to the two pathways have been referred to as the common *symbiosis* (*SYM*) genes (Kistner et al., 2005). These similarities may reflect common mechanisms for host plant cells to respond to symbionts, although the commonality is not globally defined yet.

¹ This work was supported by the Basic Science Research Program through the National Research Foundation of Korea funded by the Ministry of Education, Science, and Technology (grant no. 2-1205-0037) and by the Next-Generation BioGreen 21 Program (grant no. PJ009076012013), Rural Development Administration, Republic of Korea.

² These authors contributed equally to the article.

* Corresponding author; ccheon@sookmyung.ac.kr.

The author responsible for distribution of materials integral to the findings presented in this article in accordance with the policy described in the Instructions for Authors (www.plantphysiol.org) is: Choong-Il Cheon (ccheon@sookmyung.ac.kr).

[C] Some figures in this article are displayed in color online but in black and white in the print edition.

[W] The online version of this article contains Web-only data.

[OA] Open Access articles can be viewed online without a subscription.

www.plantphysiol.org/cgi/doi/10.1104/pp.113.215020

Plant carotenoids are mostly C₄₀ tetraterpenoid pigments with a series of double bonds (DellaPenna and Pogson, 2006; Lu and Li, 2008). They play essential roles in photosynthesis. The phytohormone abscisic acid (ABA) is synthesized from xanthophylls, oxygenated derivatives of carotenoids. The beneficial effects of carotenoids for human disease prevention and health promotion are well established and are based on their antioxidant activities (Kopsell and Kopsell, 2006; Rao and Rao, 2007; von Lintig, 2010). Metabolic engineering approaches have produced crop plants with enhanced carotenoid contents and improved nutritional value (Giuliano et al., 2008). For example, enhancement of β -carotene, provitamin A, by engineering the carotenoid biosynthetic pathway resulted in the development of cv Golden rice (*Oryza sativa*; Ye et al., 2000; Paine et al., 2005; Ha et al., 2010).

The initial step of carotenoid biosynthesis is the production of phytoene by the enzyme phytoene synthase (Fig. 1; DellaPenna and Pogson, 2006; Cazzonelli and Pogson, 2010). The subsequent activities of desaturases, isomerase, and cyclase convert phytoene into lycopene and further into β -carotene. Xanthophyll synthesis begins with the action of β -carotene hydroxylase (BCH) on β -carotene, producing initially β -cryptoxanthin and thereafter zeaxanthin (Kim et al., 2009). Overexpression of BCH has been found to confer tolerance to light stress (Davison et al., 2002). The subsequent steps catalyzed by zeaxanthin epoxidase (ZEP) and neoxanthin synthase lead to the synthesis of ABA (Takaichi and Mimuro, 1998).

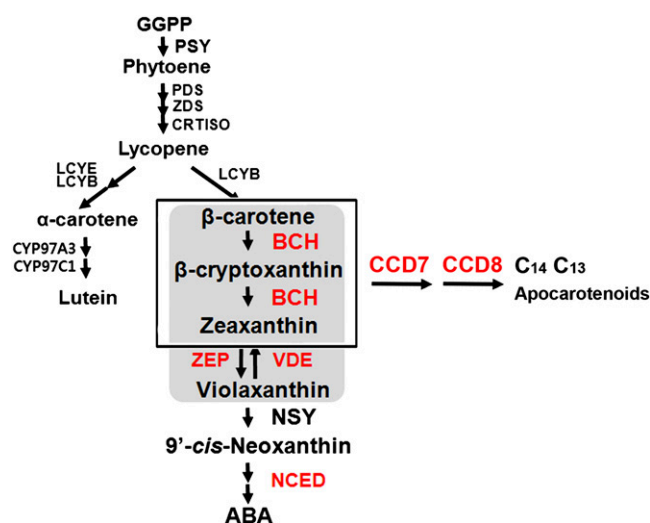


Figure 1. The biosynthetic pathway of carotenoids in plants. GGPP, Geranylgeranyl diphosphate; PSY, phytoene synthase; PDS, phytoene desaturase; ZDS, ζ -carotene desaturase; CRTISO, carotene isomerase; LCYB, lycopene β -cyclase; CYP97A3 and CYP97C1, cytochrome P450 enzymes; NSY, neoxanthin synthase; LCYE, lycopene ϵ -cyclase; CRTR-E, ϵ -carotene hydroxylase. Enzymes in red were examined in this study.

Various carotenoid cleavage dioxygenases (CCDs) catalyze the formation of apocarotenoids with functions as hormones, flavors, and pigments (Auldridge et al., 2006b; Strack and Fester, 2006; Tsuchiya and McCourt, 2009; Walter et al., 2010). Recently, CCD7 and CCD8 were shown to control the synthesis of strigolactones, newly discovered hormones that inhibit shoot branching (Gomez-Roldan et al., 2008; Umehara et al., 2008; Vogel et al., 2010; Ruyter-Spira et al., 2013). In addition, carotenoid cleavage products have been discovered in plant roots colonized by AM fungi (Strack and Fester, 2006). During AM symbiosis, roots synthesize apocarotenoids at the same time as activating plant genes for carotenoid metabolism. Although RNA interference (RNAi)-mediated inhibition of apocarotenoid synthesis suggests that apocarotenoids are functionally significant (Snowden et al., 2005; Floss et al., 2008), their role in AM symbiosis is unknown.

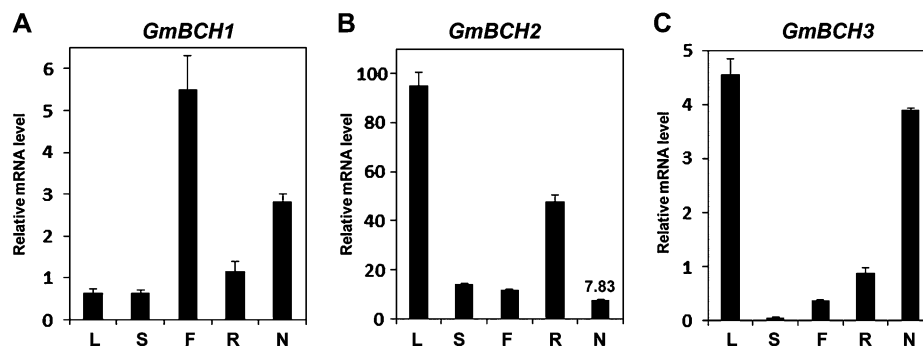
In a search for genes differentially induced during soybean (*Glycine max*)-*Rhizobium* spp. symbiosis, several antioxidant genes, including a gene encoding a putative BCH, were identified. In this report, we describe genes (*GmBCHs*) encoding a putative BCH whose expression increased in soybean root nodules. Therefore, the biochemical activities of BCHs were investigated. RNAi inhibition of *GmBCH* expression interfered with nitrogen fixation as well as nodule development. Subsequent analysis of the expression and biochemical activities of *GmCCDs* in root nodules led us to hypothesize that *GmCCD8* could be involved in the synthesis of apocarotenoids from zeaxanthin in these nodules.

RESULTS

Expression of Genes Encoding Putative BCHs in Soybean

We isolated from root nodules of soybean a complementary DNA (cDNA) with strong homology to BCH (*GmBCH1*), whose expression was higher in nodules than in roots (Fig. 2A; Lee et al., 2005). In a BLAST search with the *GmBCH1* sequence against the soybean genome (<http://www.phytozome.net/soybean.php>; Schmutz et al., 2010), we found several open reading frames encoding products with amino acid sequences highly homologous to that of *GmBCH1*; they were designated *GmBCH2* to *GmBCH5* (GenBank accession numbers are as follows: *GmBCH1* [AY575953], *GmBCH2* [BT093388], *GmBCH3* [BT098487], *GmBCH4* [JF970190], *GmBCH5* [JF970191]). The open reading frames of *GmBCH1* and *GmBCH2* are very similar to functionally confirmed BCHs (e.g. they have 74% and 75% sequence identity, respectively, to the BCH from coffee [*Coffea arabica*], CaCRTR-B; Simkin et al., 2008; Supplemental Fig. S1A). They have divergent N-terminal regions, like most previously reported BCHs, but carry four His-containing motifs, in which the spacing of the His residues was conserved (e.g.

Figure 2. Expression of the soybean BCHs *GmBCH1*, *GmBCH2*, and *GmBCH3* in soybean tissues, including 27-d-old nodules. Transcript levels were determined by real-time RT-PCR and normalized with the geometric mean of three reference genes (*GmELF1b*, *GmActin2/GmActin7*, and *Ubiq-uitin*; Vandesompele et al., 2002). Data are representative of three independent experiments. Error bars represent SD ($n = 3$). L, Leaf; S, stem; F, flower; R, root; N, nodule.



HXXXXH and HXXHH). The presence of the His residues in these motifs has been confirmed to be essential for the enzymatic activity, as mutagenesis abolishing these His residues resulted in no enzymatic conversion of β -carotene into zeaxanthin (Supplemental Fig. S1A; Bouvier et al., 1998). *GmBCH2* appears to possess a plastid transit sequence (see below; Yu et al., 2007), and *GmBCH3* has a sequence almost identical to *GmBCH1* except for its N-terminal 33 amino acids, so it also contains the above-mentioned motifs common to BCHs. The 5' untranslated regions of *GmBCH1* and *GmBCH3* differ. Whereas the *GmBCH3* locus could be identified in the present version of the soybean genome database, the unique 5' region of the *GmBCH1* sequence was not detected in the database. Therefore, we attempted to establish the presence of *GmBCH1* in the soybean genome by cloning its specific 5' DNA region (see "Materials and Methods"). A 432-bp DNA fragment, which included the upstream promoter region of *GmBCH1*, was cloned (Supplemental Fig. S2A), and this 5' region as well as the coding region of *GmBCH1* were also detected by genomic PCR (Supplemental Fig. S2B, lanes 3 and 6). *GmBCH4* and *GmBCH5* also contain the motifs mentioned above and thus are regarded as additional BCH paralogs (Supplemental Fig. S1A).

We investigated the expression of the *GmBCHs* in various tissues by real-time reverse transcription (RT)-PCR. To optimize the PCR, we examined critical aspects of the primers (Supplemental Fig. S3). The expression of *GmBCH2* was higher than that of *GmBCH1* and *GmBCH3* in most tissues, particularly in leaf, and relatively low in nodules, whereas expression of *GmBCH1* and *GmBCH3* was high in leaf and flower and noticeable in root nodules (Fig. 2). Expression of *GmBCH4* and *GmBCH5* was high in leaf and quite low in roots and nodules. These results generally match with the RNA-Seq Atlas data (Libault et al., 2010; Severin et al., 2010; Supplemental Table S1). *GmBCH3* expression in the transcriptomic data might actually reflect the expression of both *GmBCH1* and *GmBCH3*, because the coding regions of both genes are almost identical and *GmBCH1* is not identified in the current version of the soybean genome database (Supplemental Table S1).

In order to examine *GmBCH* expression during nodulation, we performed real-time RT-PCR and in

situ hybridization. For the in situ hybridization, specific regions of each gene were used to make probes for *GmBCH1/GmBCH3* and *GmBCH2* (Supplemental Figs. S1 and S4, A and B; see "Materials and Methods"). The probes were checked for hybridization specificity by whole-mount in situ hybridization to young leaves (Supplemental Fig. S4, C and D). The relative expression levels of *GmBCH1/GmBCH3* and *GmBCH2* obtained from whole-mount in situ hybridization in young leaves were found to be comparable to those from the real-time RT-PCR in Figure 2, implying that the *GmBCH* probes are not likely to cross hybridize. Sections from nodules at different stages of development were hybridized with a probe for *GmBCH1/GmBCH3* together, as they have almost identical DNA sequences. *GmBCH1* and *GmBCH3* were found to be induced as nodules matured, suggesting that both are involved in the nodulation process (Fig. 3, A, C, and D–G). Their expression was seen in the root pericycle in the early stages of nodulation and became high in the central infected zones in the early and mature nodule stages. *GmBCH2* was also expressed during nodulation, especially strongly in 7-d-old nodules (Fig. 3, B and I–L). Its expression was also strong in the root pericycle. The *GmBCH* expression levels during nodulation were confirmed by the fluorometric measurement of GUS activities using transgenic roots and nodules expressing *GmBCH2/GmBCH3* promoter (1.6-kb upstream regions of each)-GUS fusions (Supplemental Fig. S5). These observations could mean that expression of the putative BCH genes, especially *GmBCH1*, *GmBCH2*, and *GmBCH3*, may be involved in nodulation.

Enzymatic Activities of *GmBCHs*

The similarity of *GmBCH1*, *GmBCH2*, and *GmBCH3* to BCHs of other plants prompted us to test whether they were functionally active in converting β -carotene into zeaxanthin. *Escherichia coli* carrying pACCAR16 Δ crtX for the production of β -carotene (Misawa et al., 1990) was transformed with *GmBCH1* or *GmBCH2* cDNA cloned in pUC19 (p*GmBCH1* or p*GmBCH2*) or with pUC19 alone as a negative control. While HPLC analysis of the carotenoids extracted from *E. coli* transformed with pUC19 alone identified only β -carotene (Fig. 4A), *E. coli*

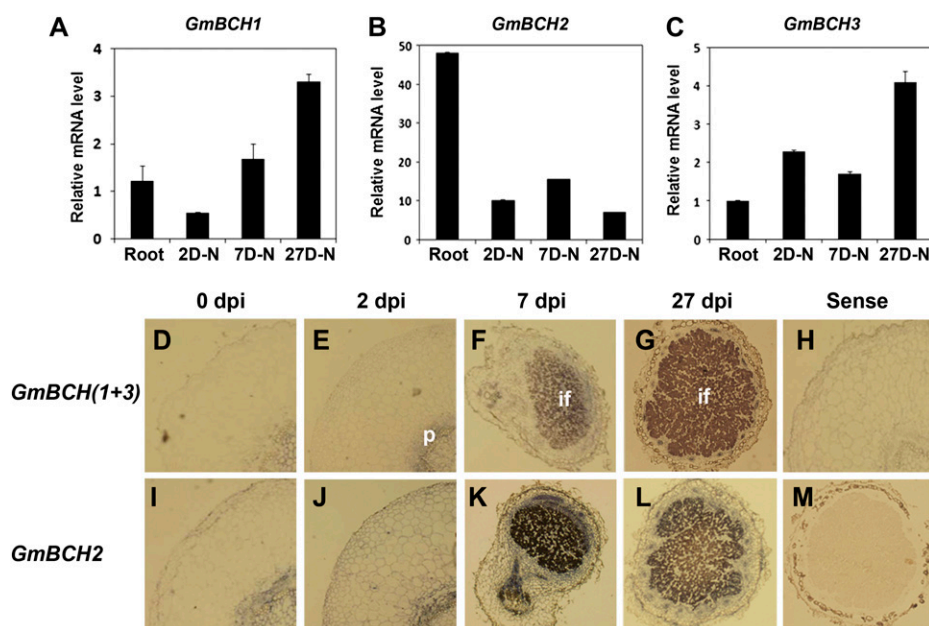


Figure 3. Expression of *GmBCHs* during nodulation. A to C, Expression of *GmBCH1* (A), *GmBCH2* (B), and *GmBCH3* (C) during nodule development. Transcript levels were determined by real-time RT-PCR and normalized. Expression levels are shown as means and SD of three independent experiments. 2D-N, Two-day-old nodule; 7D-N, 7-d-old nodule; 27D-N, 27-d-old nodule. D to M, In situ hybridization of *GmBCHs* during nodule development. Sections from 0 (roots), 2, 7, and 27 d post inoculation (dpi) were hybridized with antisense *GmBCH(1+3)* (D–G) and *GmBCH2* (I–L) riboprobes. Sections from 0 (roots) and 27 dpi were hybridized with sense *GmBCH(1+3)* (H) and *GmBCH2* (M) riboprobes as negative controls. if, Infected region; p, Pericycle.

transformants harboring the *GmBCH* genes yielded β -cryptoxanthin and zeaxanthin, as defined by their retention times and the absorption spectra of the eluents, as well as their relative molecular masses measured by liquid chromatography/mass spectrometry (MS; Fig. 4, B and C). This indicates that *GmBCH1* and *GmBCH2* convert β -carotene into β -cryptoxanthin and further into zeaxanthin (see “Discussion”). In addition, enzymatic activity of *GmBCH3* was confirmed by expressing it in *E. coli* (Fig. 4D).

Subcellular Localization of *GmBCHs*

We predicted the subcellular locations of *GmBCH1*, *GmBCH2*, and *GmBCH3* using ChloroP version 1.1 (<http://www.cbs.dtu.dk/services/ChloroP/>). *GmBCH2* and *GmBCH3* were predicted to contain a chloroplast transit peptide at its N terminus, as expected (amino acids 1–47), whereas *GmBCH1* was not. To determine the location of the enzymes experimentally, *GmBCH1*, *GmBCH2*, and *GmBCH3* cDNAs were fused with *GFP*, a reporter gene, under the control of the cauliflower mosaic virus (CaMV) 35S promoter, and the resulting constructs were introduced into *Arabidopsis thaliana* protoplasts. As predicted, the *GFP* signals from the *GmBCH2-GFP* and *GmBCH3-GFP* fusions were mainly found in plastids, whereas those of the *GmBCH1-GFP* fusion appeared to be cytosolic (Fig. 5, A–D). Deletion of the putative cleavage site in the transit peptide in the N-terminal region of *GmBCH2* resulted in cytosolic localization of the product (Supplemental Fig. S6A). Moreover, addition of the transit peptide of *GmBCH2* to the N terminus of *GmBCH1* resulted in localization of most of the *GmBCH1* to plastids, suggesting that the cytosolic localization of *GmBCH1* is not an artifact of overexpression (Supplemental Fig. S6B).

The subcellular locations of the *GmBCHs* were further examined by electron microscopic (EM) immunogold labeling with an anti-*GFP* antiserum and ultrathin sections of soybean nodules expressing *GmBCH1-GFP*, *GmBCH2-GFP*, or *GmBCH3-GFP*. Immunogold particles were detected in the cytosol of nodules expressing *GmBCH1-GFP* and in the plastids of nodules expressing *GmBCH2-GFP* and *GmBCH3-GFP* (Fig. 5E), which is consistent with the localizations reported in *Arabidopsis* protoplasts as well as the predictions obtained using ChloroP version 1.1. We used the exact binomial test in order to determine whether gold particles were preferentially located in a specific organelle (Conover, 1971). For *GmBCH1*, more than 78% of the gold particles were found in the cytosol ($P = 0.0478$). For *GmBCH2/GmBCH3*, more than 64%/70% of the gold particles were found in the plastid ($P = 0.0492/0.0329$, respectively). These results suggest that *GmBCH2* and *GmBCH3* function in the plastids of root nodules, while *GmBCH1* resides in the cytosol, unlike other BCHs. It is not clear how a cytosolic BCH can participate in carotenoid metabolism.

Drastically Reduced Nitrogen Fixation in Nodules Expressing RNAi against *GmBCHs*

To see if *GmBCH1/GmBCH3* were essential for nodule growth, we made an RNAi construct against them and subcloned it downstream of the leghemoglobin (*Lbc3*) promoter. This RNAi construct contained a part of the N-terminal region of *GmBCH1* and *GmBCH3* that includes the 5' untranslated region of *GmBCH3* (Supplemental Fig. S7). The sequence of the RNAi construct was 99% identical to *GmBCH1* and *GmBCH3* and had significant identity to *GmBCH4* but not to *GmBCH2* or *GmBCH5*. The resulting cassette, *GmBCH*

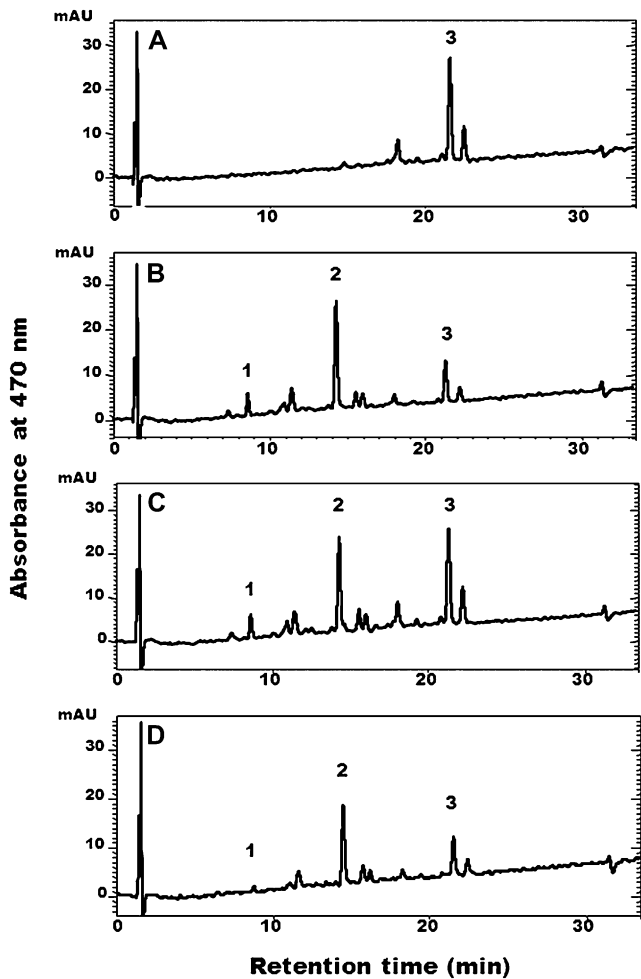


Figure 4. HPLC analysis of carotenoids extracted from β -carotene-producing *E. coli* transformed with *GmBCH1*, *GmBCH2*, or *GmBCH3*. pACCAR16 Δ ctX-containing *E. coli* harboring pUC19 alone as a negative control (A) or harboring pGmBCH1 (B), pGmBCH2 (C), or pGmBCH3 (D) was used for carotenoid analysis. Peak 1, Zeaxanthin; peak 2, β -cryptoxanthin; peak 3, β -carotene. mAU, Milliabsorbance units.

(1+3)-RNAi, was introduced into pCAMBIA1304, which harbors 35S-*GUS* (the CaMV 35S promoter fused to *GUS*) as a reporter. This construct was introduced into *Agrobacterium rhizogenes* to generate transgenic hairy roots (Lee et al., 2005).

The formation of root nodules was markedly reduced on the *GmBCH*(1+3)-RNAi hairy roots (Fig. 6A), and similar defective nodulation was observed when a transgenic hairy root formed along with a non-transgenic (*GUS*-negative) hairy root on the same plant (Fig. 6B). In the meantime, there appeared to be no difference in root growth between the transgenic and nontransgenic hairy roots. The impairment of nodulation on *GmBCH*(1+3)-RNAi hairy roots resulted in lower nodule weight, as measured in 24 *GmBCH*(1+3)-RNAi plants and 19 controls (Fig. 6C). When we checked the expression levels of *GmBCH1* and

GmBCH3 in the transgenic nodules, we found that these varied; hence, as representatives with different nodule weights, we chose RNAi plants 2, 20, and 21 for further expression analysis. RNAi plants 20 and 21, as expected, had significantly reduced expression of *GmBCH1* and *GmBCH3* together with decreased nodule weights (RNAi type 2), whereas *GmBCH1* and *GmBCH3* expression was less affected in the RNAi plants, with almost the same nodule weights as the control, such as RNAi plant 2 (RNAi type 1; Fig. 6D). Although the relationship between the expression

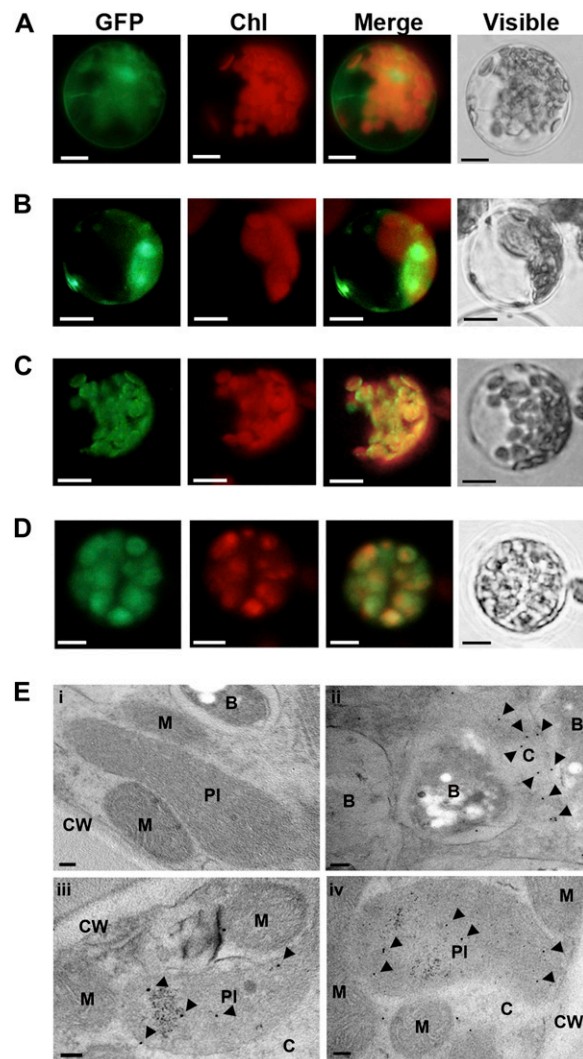


Figure 5. Subcellular localization of GmBCHs in Arabidopsis protoplasts and soybean nodules. A to D, Arabidopsis protoplasts were transfected with control vector (35S-GFP; A), *GmBCH1*-GFP (B), *GmBCH2*-GFP (C), or *GmBCH3*-GFP (D). Bars = 10 μ m. E, GmBCHs were localized by EM immunogold labeling with an anti-GFP antiserum in soybean nodules transformed with empty vector (pCAMBIA3301; i), *GmBCH1*-GFP (ii), *GmBCH2*-GFP (iii), or *GmBCH3*-GFP (iv). Gold particles (10 nm) are indicated by arrowheads. B, Bacteroids; C, cytoplasm; CW, cell wall; M, mitochondria; PI, plastid. Bars = 100 nm.

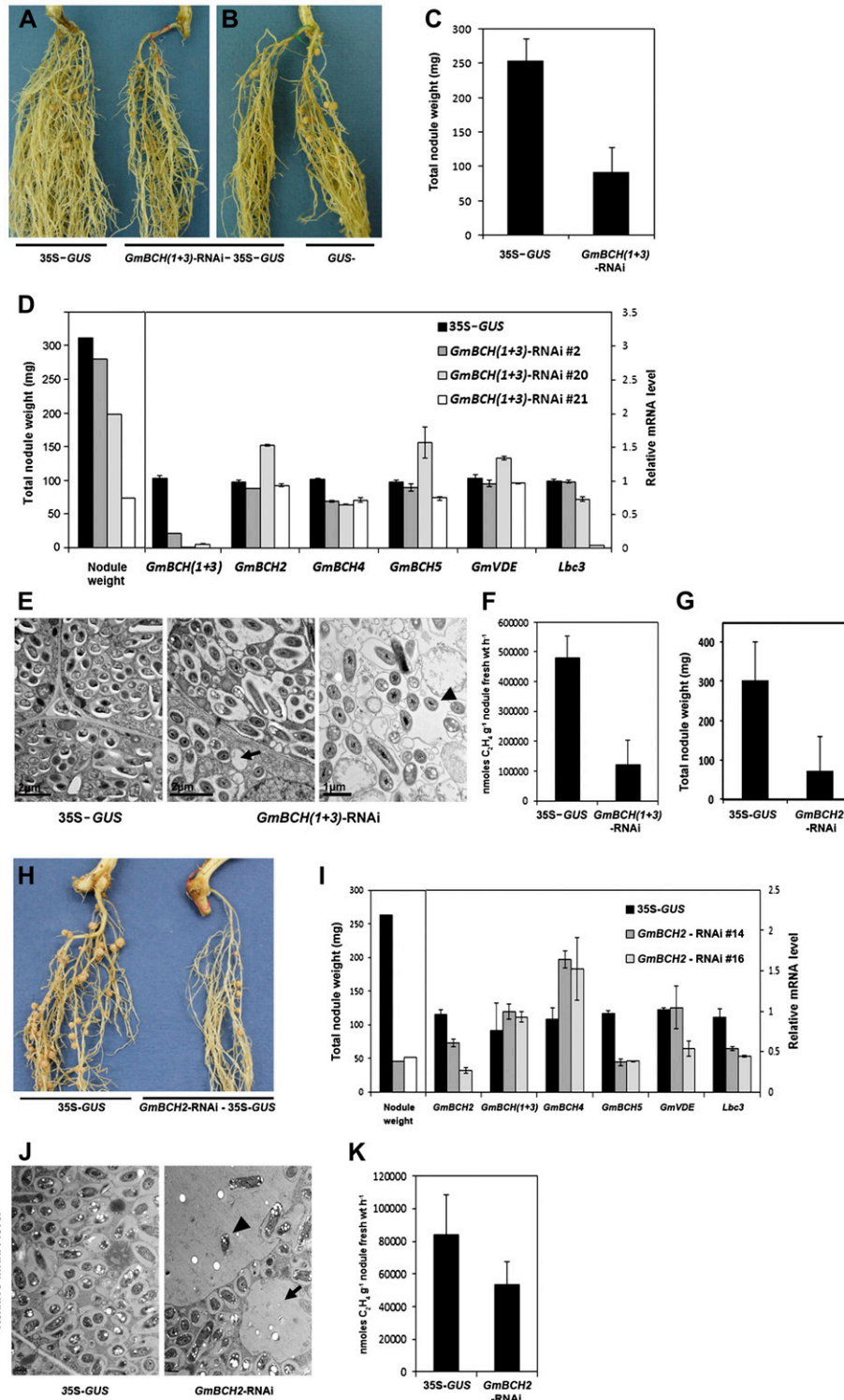


Figure 6. Nodule development on transgenic hairy roots expressing an RNAi construct against both *GmBCH1* and *GmBCH3*. A, Nodules formed on transgenic hairy roots containing pCAMBIA1304 alone (control; 35S-GUS; left plant) or the *GmBCH(1+3)*-RNAi cloned in pCAMBIA1304 (right plant). After GUS assay, only GUS-positive (transgenic) hairy roots were inoculated with *B. japonicum* (K599). These experiments were repeated three times, and representative results are shown. In each experiment, five to seven plants were used per construct. B, A GUS-negative (untransformed control) hairy root is shown on the right. C, Total nodule weights (mg) of control (35S-GUS) and *GmBCH(1+3)*-RNAi plants were measured and are shown as means and SD of three independent experiments. D, Transcript levels are shown in nodules from a transgenic control plant (35S-GUS) and

levels of *GmBCH(1+3)* and nodule weight is only shown for the three representative transgenic plants (i.e. 2, 20, and 22) in Figure 6D, we actually examined the expression levels and nodule weights in 12 transgenic plants and four controls.

To establish the statistical significance of the RNAi plant groups (i.e. control versus RNAi type 1 versus RNAi type 2), we conducted an ANOVA with Tukey's multiple comparison procedure and found significant differences in nodule weight between control and RNAi type 2 as well as between RNAi type 1 and RNAi type 2 (Supplemental Fig. S8A); there was also a significant difference in the expression of *GmBCH(1+3)* between these pairs (Supplemental Fig. S8B; Maritz, 1981). In addition, using all 16 plants making up the three groups, we examined the correlation between gene expression level and nodule weights based on the Spearman rank correlation coefficient. This yielded a strong positive correlation of 0.76 ($P = 0.001$; Supplemental Fig. S8C). Meanwhile, *GmBCH4* expression, which was quite low in root nodules, was somewhat affected in most of the RNAi plants. The expression of *GmBCH2* as well as *GmBCH5* was not altered in any of the plants (Fig. 6D). These observations imply that the effect of the RNAi on *GmBCH* transcript levels was specific to *GmBCH1* and *GmBCH3*. Expression of *GmVDE*, a gene contributing positively to the accumulation of zeaxanthin from the opposite direction of *GmBCH* in the xanthophyll cycle (Fig. 1; Cazzonelli and Pogson, 2010), was also unaffected, indicating that silencing of the *GmBCHs* in the RNAi nodules was not compensated, at least at the transcription level, by the induction of *GmVDE* (Fig. 6D). In agreement with the observed retardation of nodule development, on the other hand, expression of *Lbc3*, which encodes leghemoglobin, an oxygen carrier for symbiosis with rhizobia that is one of the hallmark genes for the development of nitrogen-fixing nodules (Ott et al., 2005), was decreased in RNAi plants 20 and 21 (Fig. 6D). In addition, acetylene reduction assays showed that nitrogen-fixing ability was also lower in the RNAi nodules (Fig. 6F). The RNAi nodules

examined by electron microscopy contained empty vesicles rather than symbiosomes with rhizobia in about 60% of the cells examined. In addition, the rhizobia were not even enclosed by symbiosome membranes in about 5% of the cells of the RNAi nodules with strongly repressed *GmBCH(1+3)* (Fig. 6E; Supplemental Fig. S9). These data indicate that the expression of *GmBCH1* and/or *GmBCH3* may be essential for nodule development.

Expression of *GmBCH2* was prominent during nodulation; hence, we also silenced *GmBCH2* in nodules using the leghemoglobin promoter-driven RNAi approach. When we compared nine *GmBCH2*-RNAi plants with eight control plants, we found that the reduction in *GmBCH2* expression resulted in decreased nodule weight and nitrogenase activity (Fig. 6, G–K). *GmBCH5* expression was also reduced in the *GmBCH2*-RNAi nodules, probably due to its strong homology with *GmBCH2*, while the expression of *GmBCH1* and *GmBCH3* was not affected and *GmBCH4* expression was somewhat increased (Fig. 6I). About 65% of the infected cells examined contained empty vesicles, and most of them exhibited the presence of bacteroids outside symbiosomes (Fig. 6J). It is not clear whether the phenotypic difference observed by electron microscopy of *GmBCH(1+3)*-RNAi nodules and *GmBCH2*-RNAi nodules indicates their different roles in nodulation. In addition, the expression of *GmBCH4* and *GmBCH5* was also observed in nodules, albeit at a low level (Supplemental Fig. S1, B and C). Taken together, these results suggest that the *GmBCHs*, comprising *GmBCH1* to *GmBCH5*, may be essential for nodule development.

Decreased Expression of the Putative Zeaxanthin Epoxidase Gene during Nodulation

The impairment of nodulation in the RNAi hairy roots suggested to us that a product of BCH action, or some other derivatives of the carotenoid metabolic pathway, plays an important role in nodulation. This led us to examine the expression of genes encoding

Figure 6. (Continued.)

three representative transgenic plants: *GmBCH(1+3)*-RNAi 2, *GmBCH(1+3)*-RNAi 20, and *GmBCH(1+3)*-RNAi 21. RNAi plant 2 had almost the same nodule weight as the control, RNAi plant 20 had a reduced nodule weight, and RNAi plant 21 had a drastically reduced nodule weight. Transcript levels of *GmBCH(1+3)*, *GmBCH2*, *GmBCH4*, *GmBCH5*, *GmVDE*, and *Lbc3* were determined by real-time RT-PCR in controls (35S-*GUS*) and three *GmBCH(1+3)*-RNAi nodules and normalized. Expression levels are shown as means and SD of three independent experiments. E, EM images of 27-d-old control (35S-*GUS*) and *GmBCH(1+3)*-RNAi plants. *GmBCH(1+3)*-RNAi nodules often contained empty vesicles (arrow) and bacteroids outside the symbiosomes (arrowhead). F, Nitrogenase activities were measured by the acetylene reduction assay, and data are averaged from three independent experiments. G, Total nodule weights (mg) of control (35S-*GUS*) and *GmBCH2*-RNAi plants were measured and are shown as means and SD of three independent experiments. H, Nodules formed on transgenic hairy roots containing pCAMBIA1304 alone (control; 35S-*GUS*; left plant) or the *GmBCH2*-RNAi cloned in pCAMBIA1304 (right plant). After GUS assay, nodules were formed as in A. I, Transcript levels in nodules from one transgenic control plant (35S-*GUS*) and two differentially repressed transgenic plants (*GmBCH2*-RNAi 14 and *GmBCH2*-RNAi 16) are shown. Transcript levels of *GmBCH2*, *GmBCH(1+3)*, *GmBCH4*, *GmBCH5*, *GmVDE*, and *Lbc3* were determined by real-time RT-PCR and normalized. Expression levels are shown as means and SD of three independent experiments. J, EM images of 27-d-old control (35S-*GUS*) and *GmBCH2*-RNAi nodules. *GmBCH2*-RNAi nodules often contained empty vesicles (arrow) and bacteroids outside the symbiosomes (arrowhead). K, Nitrogenase activities were measured by the acetylene reduction assay as in F.

two enzymes of the xanthophyll cycle: ZEP and violaxanthin deepoxidase (VDE). Since we identified three *GmZEPs* (Supplemental Fig. S1D) and two *GmVDEs* (Supplemental Fig. S1E) in the soybean genome sequence, we examined their expression. Actually, we came across a few more DNA sequences homologous to the *ZEP* and *VDE* genes in other plants, but they showed only partial identity and were not further studied (Supplemental Fig. S1, D and E). The primers used to examine the expression of *GmZEPs* and *GmVDEs* were designed using DNA sequences highly conserved among other plants. The transcript levels of both genes were considerably lower in roots and nodules than in the aerial parts of the plant, such as leaves, stems, and flowers (Fig. 7, A and B; Supplemental Fig. S10). As nodules matured, *GmZEP* expression decreased and was almost undetectable in mature 27-d-old nodules (Fig. 7D). Expression of the *GmVDEs* remained relatively constant throughout nodule development (Fig. 7E). In addition, we examined the expression of two soybean 9-cis-epoxycarotenoid dioxygenase1 (*NCED1*) orthologs (*GmNCED1a* and *GmNCED1b*; Supplemental Fig. S1F) and found that their expression was high in flowers but quite low in roots and nodules, although expression in 7-d-old nodules was a little higher than in other stages of nodulation (Fig. 7, C and F). The expression levels of *GmZEPs*, *GmVDEs*, and *GmNCED1s* generally matched with those in the soybean RNA-Seq Atlas, especially expression in the aerial parts of the soybean (Libault et al., 2010; Severin et al., 2010; Supplemental Table S1). These expression data appear to indicate that *GmZEPs*, *GmVDEs*, and *GmNCED1s* do not play

major roles, if any, in further carotenoid metabolism after BCH during nodulation, although we cannot rule out the possibility that their protein levels are higher than suggested by their transcript levels.

Expression of CCDs in Soybean Root Nodules

We hypothesized that zeaxanthin might be synthesized in root nodules by BCHs and converted to other carotenoids, although not via xanthophyll to ABA, because *ZEP* expression was very low (Fig. 7D). Therefore, we extracted and quantified carotenoids from root nodules. Contrary to our expectation, carotenoids including zeaxanthin were almost undetectable in root nodules (data not shown). This raised the question of what biochemical reactions occur in root nodules subsequent to zeaxanthin production by the BCHs. Since carotenoid cleavage products have been found in roots infected with mycorrhizal fungi and are regarded as important in AM symbiosis (Strack and Fester, 2006), we reasoned that the carotenoids synthesized in root nodules might be depleted if CCDs were active. The white-colored petals of *Chrysanthemum* spp. express high levels of *CmCCD4a*, with the result that no carotenoid can be detected (Ohmiya et al., 2006), and RNAi-mediated suppression of *CmCCD4a* expression was found to lead to the accumulation of carotenoids and yellow petal color, confirming the relationship between the amount of carotenoid and the expression of *CmCCD4a*. Thus, we considered the possibility that the conversion of carotenoids into apocarotenoids by CCDs might explain our failure to detect carotenoids in root nodules.

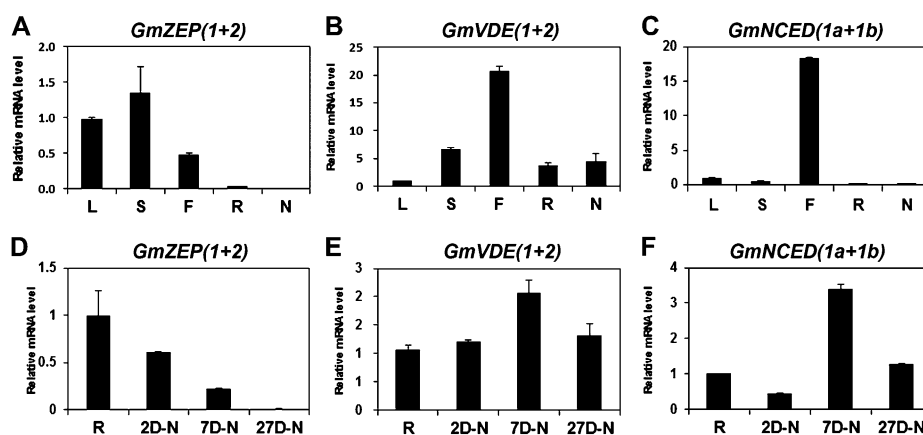


Figure 7. Expression of *GmZEPs*, *GmVDEs*, and *GmNCED1s* in soybean. A to C, Expression of *GmZEPs*, *GmVDEs*, and *GmNCED1s* in different tissues. RNA was extracted from different tissues, including 27-d-old nodules of soybean. D to F, Expression of *GmZEPs*, *GmVDEs*, and *GmNCED1s* during nodule development. RNAs were extracted from roots and 2-, 7-, and 27-d-old nodules, and transcript levels were determined by real-time RT-PCR and normalized. Expression of *GmZEP1* and *GmZEP2* was examined simultaneously using primers for DNA regions of high identity, while the expression of *GmZEP3*, a gene with low overall homology to other *GmZEPs*, was measured separately and is shown in Supplemental Figure S10. Expression of *GmVDE1* and *GmVDE2* was also examined simultaneously using primers for the DNA regions of high identity. Expression of *GmNCED1a* and *GmNCED1b* was also examined simultaneously using primers for the DNA regions of high identity. Data are from three independent experiments. L, Leaf; S, stem; F, flower; R, root; N, nodule; 2D-N, 2-d-old nodule; 7D-N, 7-d-old nodule; 27D-N, 27-d-old nodule.

We tested this possibility by examining the expression of CCDs in root nodules of soybean. We chose to examine the expression of *CCD1*, *CCD7*, and *CCD8* in nodules and excluded *CCD4* due to its primary expression in aerial tissues. From the soybean genome sequence (<http://www.phytozome.net/soybean.php>), we obtained the DNA sequences of putative versions of *CCD7* and *CCD8*, which are reported to cleave carotenoids. The deduced amino acid sequences of *CCD7* and *CCD8* (designated *GmCCD7* and *GmCCD8* hereafter) were very similar to previously reported *CCD7* and *CCD8* sequences and were named *GmCCD7a*, *GmCCD7b*, *GmCCD8a*, and *GmCCD8b* (Supplemental Fig. S1, G and H). In addition, we also encountered putative *GmCCD1a* and *GmCCD1b* sequences and examined their expression (Supplemental Fig. S1I). We found a few more DNA sequences, but their deduced amino acid sequences were only partially identical to previously reported CCDs and not studied further (Supplemental Fig. S1, G and H). Using appropriate primers, the expression of *GmCCD7s* and *GmCCD8s* proved to be relatively high in roots and nodules, whereas *GmCCD1* expression was seen in all tissues, in agreement with previous data (Libault et al., 2010; Severin et al., 2010; Fig. 8, A–C; Supplemental Table S1). Although the expression of *GmCCD7s* was rather low, it, as well as that of *GmCCD8s*, appeared to be induced upon rhizobial infection (Fig. 8, E and F).

Therefore, we tested whether *GmCCD7*/*GmCCD8* could actually cleave zeaxanthin. *E. coli* transformed with zeaxanthin biosynthetic genes cloned in the vector pACYC184 (pAC-zeaxanthin) produced zeaxanthin, as shown by HPLC analysis as well as by the yellow color of colonies (Fig. 9, A and B). *GmCCD7a*-expressing *E. coli* was also yellow, and a protein of the expected size corresponding to *GmCCD7* (70 kD) was detected by SDS-PAGE (Fig. 9C), but lysates gave a strong peak of zeaxanthin, implying that the zeaxanthin produced

was not cleaved. In contrast, *E. coli* transformed with the *GmCCD8a*-expressing plasmid was no longer yellow while producing a protein of the expected mass (60 kD). This recombinant *E. coli* strain gave only a very small zeaxanthin peak (Fig. 9, A and B, asterisks). The integrity of *GmCCD7a* was also tested by another *E. coli* functional assay, in which the β -carotene-cleaving activity of *GmCCD7* was examined and compared with other CCDs in *E. coli* carrying the plasmid pACCAR16 Δ crtX that enables the accumulation of β -carotene (Supplemental Fig. S11). β -Carotene-cleaving activity was consistently detected in *GmCCD7a*-expressing *E. coli*, although it was about 3-fold lower than that of an *AtCCD7*-expressing *E. coli* (Supplemental Fig. S11, C and D). Moreover, the apparent gap in the activity between *GmCCD7a* and the other two CCDs in this assay (Supplemental Fig. S11, C–E) could be further reduced if the relative protein expression level of these proteins was taken into account, as measured by western blots of these cell extracts (Supplemental Fig. S11A). Therefore, it seems likely that both *GmCCD7a* and *GmCCD8a* are functional enzymes involved in β -carotene metabolism in soybean nodules. These data also imply that zeaxanthin is cleaved by *GmCCD8a* but not by *GmCCD7a*, although we cannot exclude the possibility that *GmCCD7a* synthesized in root nodules may have cleavage activity on zeaxanthin. Taken together, our observations suggest that carotenoids such as zeaxanthin are synthesized but are cleaved by *GmCCD8* during soybean nodule development.

DISCUSSION

We have investigated the significance of carotenoid metabolism in nodule development. This work was prompted by the isolation of a gene encoding BCH as a

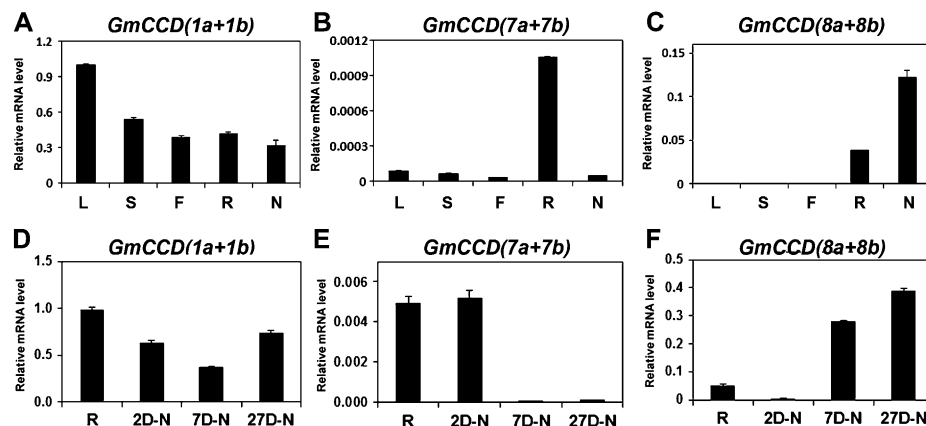


Figure 8. Expression of *GmCCDs* in soybean. A to C, Expression of *GmCCD1s*, *GmCCD7s*, and *GmCCD8s* in different tissues. RNA was extracted from various tissues, including 27-d-old nodules of soybean. D to F, Expression of *GmCCD1s*, *GmCCD7s*, and *GmCCD8s* during nodulation. RNAs were extracted from roots and 2-, 7-, and 27-d-old nodules, and transcript levels were determined by real-time RT-PCR and normalized. Expression levels are shown as means of three independent experiments. L, Leaf; S, stem; F, flower; R, root; N, nodule; 2D-N, 2-d-old nodule; 7D-N, 7-d-old nodule; 27D-N, 27-d-old nodule.

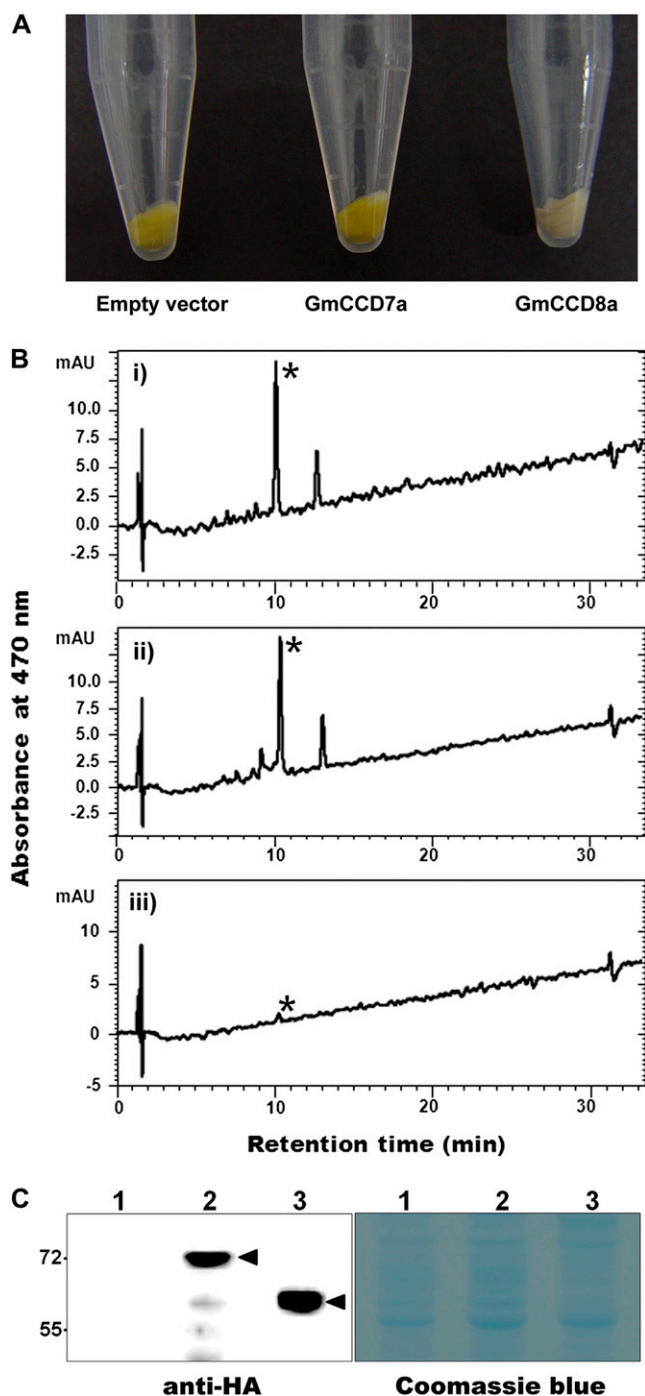


Figure 9. Functional assays of GmCCD7 and GmCCD8 in *E. coli*. **A**, Expression of *GmCCD7a* (middle) or *GmCCD8a* (right) in *E. coli* strains that carry pAC-zeaxanthin and accumulate zeaxanthin. A zeaxanthin-accumulating *E. coli* strain with empty vector alone (left) served as a negative control. **B**, HPLC analysis of carotenoids extracted from zeaxanthin-accumulating *E. coli* cells expressing *GmCCD7a* (ii) or *GmCCD8a* (iii) or with empty vector (i). The zeaxanthin peak is indicated by the asterisks. mAU, Milliabsorbance units. **C**, Proteins from zeaxanthin-accumulating *E. coli* cells expressing HA-*GmCCD7* (lane 2) and HA-*GmCCD8* (lane 3) or with empty vector (lane 1) were isolated (right panel) and immunoblotted with hemagglutinin (HA) antibody (left panel). Proteins of the expected sizes corresponding to

gene differentially expressed in root nodules (Lee et al., 2005). *GmBCH1*, *GmBCH2*, and *GmBCH3* expression was found to increase during nodulation and was especially localized to the infected region of nodules (Figs. 2 and 3). In addition, RNAi-mediated repression of these genes resulted in the retardation of nodule development, including impairment in symbiosome formation (Fig. 6; Supplemental Fig. S9). In the RNAi nodules, nitrogen fixation appeared to be damaged, judging from nitrogenase assays as well as the expression of *lbc3*, an essential gene for nitrogen fixation. We have thus presented evidence, to our knowledge for the first time, that carotenoid metabolism by GmBCHs is required for proper nodule development.

We confirmed that the GmBCHs we isolated from root nodules encoded active enzymes. cDNAs were expressed in *E. coli* harboring a vector for producing β -carotene (Misawa et al., 1990), and HPLC analyses of *E. coli* expressing the GmBCHs revealed the accumulation of zeaxanthin and also of large amounts of β -cryptoxanthin (Fig. 4). Similar results have been reported from functional assays in *E. coli* (Yu et al., 2007), while the expression of other BCH orthologs resulted in the synthesis of more zeaxanthin than cryptoxanthin (Sun et al., 1996; Galpaz et al., 2006). The synthesis of β -cryptoxanthin, that is, the asymmetric addition of hydroxyl groups to the β -end group of β -carotene, could be due to a slightly different conformation of the BCHs in *E. coli* or the failure of the BCHs to form a stable dimer (Sun et al., 1996; Yu et al., 2007). In any case, the results confirm that the putative GmBCHs are, indeed, functional BCHs.

To our surprise, we failed to detect any carotenoids in root nodules. To account for this, we tested the possibility that all the carotenoids were cleaved to synthesize ABA, since ABA is able to coordinate some aspects of nodulation (Ding et al., 2008). However, the expression of putative *GmZEPs* and putative *GmNCED1s* was found to be quite low in nodules (Fig. 7, A and C; Supplemental Fig. S10A), and furthermore, *GmZEP* expression became almost undetectable in mature nodules (Fig. 7D; Supplemental Fig. S10B), while the expression of putative *GmVDEs* in root nodules was similar to the level in roots (Fig. 7E). In fact, nodule number is decreased by ABA treatment (Suzuki et al., 2004), and a *Lotus japonicus* mutant with reduced endogenous ABA exhibited enhanced nodulation and nitrogen fixation (Tominaga et al., 2009). Since ABA was suggested to be a negative regulator of nodulation, it is possible that its concentration is not high in effective nodules. However, we cannot exclude the possibility that a certain amount of carotenoid is metabolized to ABA during specific stages of nodulation.

GmCCD7 (70 kD) and GmCCD8 (60 kD) were detected. Immunodetected bands are indicated by arrowheads. [See online article for color version of this figure.]

Despite its high sequence homology with other plant *CCD8s* (Supplemental Fig. S1H), *GmCCD8a* apparently exhibited activity on both β -carotene and zeaxanthin in our *E. coli* functional assay, contradicting the current view of substrate specificity and the proposed role for *CCD8* in the sequential cleavage reactions of C_{40} carotenoids (Alder et al., 2008; Walter et al., 2010). On the other hand, this result is consistent with an earlier report that showed direct cleavage activity of *AtCCD8* on a few C_{40} carotenoids (Auldridge et al., 2006a). In addition, it was reported that *CCD8* interfered with carotenoid biosynthesis when it was over-expressed in *E. coli* (Alder et al., 2008). Therefore, our results here, together with the previous data of Auldridge et al. (2006a), appear to suggest that more in-depth studies on the reaction catalyzed by *CCD8*, including the nature of the substrate and the cleavage product, are needed. Before drawing a conclusion that *GmCCD8a* is able to cleave zeaxanthin, it will be necessary to identify the cleavage products generated in the assay. The data in Figure 9 also show that *GmCCD7a* did not alter the HPLC profile of zeaxanthin-producing *E. coli*. Since recombinant *AtCCD7* has broad substrate specificity and cleaves C_{40} carotenoids, including β -carotene, into C_{27} and C_{13} apocarotenoids (Booker et al., 2004; Schwartz et al., 2004) and *GmCCD7* cleaved β -carotene, albeit less efficiently than *AtCCD7* (Supplemental Fig. S11), we cannot exclude the possibility that the *GmCCD7* synthesized in root nodules can cleave diverse C_{40} carotenoids, including zeaxanthin. Based on these observations, we propose that *GmCCD7*, and possibly *GmCCD8*, cleave C_{40} carotenoids and that the cleavage products are further cleaved by *GmCCD8* (Alder et al., 2008) inside nodule tissue.

The carotenoids synthesized inside the chloroplasts of leaves play essential roles in photosynthesis. On the other hand, those present in flowers, fruits, or roots are not needed for photosynthesis and accumulate in special subcellular compartments such as chromoplasts and cytoplasmic lipid vesicles. For example, a β -carotene oxygenase in a unicellular green alga (*Haematococcus pluvialis*) was localized to the lipid vesicles outside plastids (Grünewald et al., 2001). In our study, both in silico prediction and actual experiment showed that *GmBCH2* and *GmBCH3* were present in plastids, whereas *GmBCH1* was present, unexpectedly, in the cytosol (Fig. 5). Interestingly, the localization of *GmBCH1* in the cytosol seems to be closely associated with a short stretch of N-terminal sequences present only in *GmBCH1*, in addition to the putative transit-peptide sequence that is present in all of the plastidial *GmBCH* isoform sequences. Perhaps adding this sequence makes the transit peptide nonfunctional. Although no corresponding locus to *GmBCH1* was found in the soybean genome database (<http://www.phytozome.net>), we have been able to clone *GmBCH1* repeatedly by RT-PCR and also could isolate its 0.45-kb upstream sequences from cv Williams 82, from which the soybean sequence database

was generated, as well as cv Sinpaldal 2, which has been used as the material of this study, by DNA walking (Supplemental Fig. S2). Therefore, it is likely that *GmBCH1* may be present in an unsequenced gap of the present soybean genome sequence. The substrate of *GmBCH1* in the cytosol of infected cells, and the significance of its cytosolic location for the symbiotic interaction between soybean and *Rhizobium* spp., need to be studied in the future.

Carotenoid cleavage products such as β -ionone or dihydroactinidiolide are synthesized in conditions of stress, being involved in plant protection mechanisms (Bouvier et al., 2005). It is thought that the synthesis of carotenoids and their cleavage products promotes symbiosis between plants and the arbuscular mycorrhiza (Strack and Fester, 2006; Walter et al., 2010). However, since little attention has been paid to the presence of (apo)carotenoids in root nodules, it remains unclear what role the former plays in root nodule symbiosis, given that our work points to the presence of apocarotenoids as well as carotenoids in the nodules. Since nodulation and nitrogen fixation were severely inhibited in the *GmBCH-RNAi* root nodules (Fig. 6) and the expression of *GmBCHs* and *GmCCDs* was induced during nodulation, the biosynthesis of carotenoids and presumably apocarotenoids appears to play a significant role in nodulation. A possible role of carotenoid cleavage products is to protect the infected cells from oxidative stress. The symbiosomes enclosing rhizobia must produce tremendous amounts of reactive oxygen species, since a nitrogen-fixing infected cell contains about 20,000 rhizobia. Alternatively, apocarotenoids may act as signaling molecules during the maturation of nodules. A further possibility is that C_{13} and C_{14} apocarotenoids are essential for rhizobial symbiosis, as proposed for AM symbiosis (Walter et al., 2010). While there seems to be no clear indication which apocarotenoid(s) is effective in AM symbiosis, identification of the apocarotenoids present in root nodules may offer a key to understanding the establishment and functioning of legume-*Rhizobium* spp. symbiosis.

MATERIALS AND METHODS

Plants, Rhizobia, and Growth Conditions

Soybean (*Glycine max* 'Sinpaldal 2') seeds were sterilized and grown in darkness on moist, absorbent paper at 28°C for 3 d. Three-day-old seedlings were inoculated with rhizobia (*Bradyrhizobium japonicum* 'USDA110'), transferred to sterilized vermiculites, and grown at 28°C for 1 month. Tissues harvested from soybean were frozen immediately in liquid nitrogen and stored at -70°C until used for RNA extraction. For real-time PCR, mature leaves (fully expanded), stems, flowers (including flower buds and mature flowers), roots, and the mature nodule (27 d old) were collected separately.

Gene Isolation and Vector Construction

A partial cDNA clone of *GmBCH2* (BE607999) was identified by a BLAST search at the National Center for Biotechnology Information EST database. Because this clone did not contain the 5' end of the open reading frame, RACE PCR was performed to recover the missing 5' DNA sequence, and the coding

sequence was extended using the CapFishing kit (Seegene). Full-length first-strand cDNA synthesized with oligo(dT)-ACP was amplified using the primers listed in Supplemental Table S2. The degenerate primers for *GmZEP* and the primers for the full-length cDNA are shown in Supplemental Table S2 as well. To generate the constructs for bacterial expression, the coding regions of the *GmBCHs* were amplified with *Pfu* DNA polymerase (Corebio; Supplemental Table S2). Full-length cDNAs encoding the putative CCD7 and CCD8 in soybean were obtained from the soybean genome sequence (<http://www.phytozome.net/soybean.php>), and full-length *GmCCD7* and *GmCCD8* cDNAs were amplified from nodule RNA by RT-PCR (Supplemental Table S2). The resulting amplified products were cloned into pUC19 to make pGmBCH1, pGmBCH2, pGmBCH3, p3HA-GmCCD7, and p3HA-GmCCD8, and their sequences were confirmed by DNA sequencing.

A DNA fragment including the 5' region as well as the coding region of *GmBCH1* was isolated from soybean genomic DNA using the DNA Walking SpeedUP Premix Kit (Seegene). PCR was performed with an adaptor provided in the kit and the following gene-specific primers: *GmBCH1* primer, 5'-GAGAGT-GTTTGTGTTCCGCTGCG-3'; second nested *GmBCH1* primer, 5'-AGTAAGGAAT-GTGATGATCCC-3'; third nested *GmBCH1* primer, 5'-CTATCCCCCATGAA-GCGAATGCC-3'. The PCR products were cloned into the pGEM-T Easy vector (Promega) and sequenced.

To make *GmBCH* promoter-*GUS* fusions, the 5' upstream sequences of *GmBCH2* and *GmBCH3* were identified in the soybean genome (<http://www.phytozome.net/soybean.php>) as shown in Supplemental Figure S5. The 1.5-kb 5' upstream regions of *GmBCH3* and *GmBCH2* were amplified by PCR with *Pfu* DNA polymerase (Corebio) using the primers shown in Supplemental Table S2 and cloned upstream of *GUS* in pCAMBIA3301. Fluorometric assays of *GUS* activity were performed as described by Jefferson et al. (1987) with modifications.

Real-Time RT-PCR

Total RNA was extracted with the RNeasy Plant Mini Kit (Qiagen), and cDNAs were synthesized with Moloney murine leukemia virus reverse transcriptase (Promega) after treatment with DNase I to remove contaminating genomic DNA. One microliter of first-strand cDNA was used as a template, and the primers used are listed in Supplemental Table S2. Real-time RT-PCR was performed with SYBR Green PCR Master Mix (Takara) using a Rotor-Gene 3000 (Corbett Research) and the ABI Prism 5700 sequence detection system. All RT-PCR transcript levels were normalized with the geometric mean of three reference genes (*GmELF1b*, *GmActin2*/*GmActin7*, and *Ubiquitin*; Vandesompele et al., 2002).

In Situ RNA Hybridization

In situ RNA hybridization was performed according to Oh et al. (2001). Nodules were harvested 2, 7, and 27 d after rhizobial inoculation. Each nodule was processed by microtechniques, hybridized with digoxigenin-labeled antisense and sense RNA probes under standard conditions, and washed with low-stringency and high-stringency buffers for longer than under standard conditions. Hybridization stringency was established by the washing steps in order to avoid cross hybridization. The probes for *GmBCH(1+3)* and *GmBCH2* were made using the N-terminal regions of the *GmBCHs*, which have no significant sequence similarity to each other (Supplemental Fig. S4); we used a 400-bp region for the *GmBCH(1+3)* probe and a 300-bp region for the *GmBCH2* probe, as indicated in Supplemental Figure S1A. Whole-mount in situ hybridization of soybean leaves was performed with the *GmBCH(1+3)* and *GmBCH2* probes according to Weigel and Glazebrook (2002), and images from whole-mount in situ hybridization were quantified with ImageJ (National Institutes of Health) as described by Ubuka and Bentley (2009).

HPLC Analysis of Carotenoids

To measure their activities, pGmBCH1, pGmBCH2, pGmBCH3, and pUC19 as a negative control were introduced into *Escherichia coli* JM109 carrying pACCAR16ΔcrtX, which expresses genes for the production of β-carotene (Misawa et al., 1990). *E. coli* transformants were grown overnight at 28°C in 2 mL of Luria-Bertani liquid medium containing 50 μg mL⁻¹ ampicillin and 35 μg mL⁻¹ chloramphenicol. The overnight cultures were used to inoculate 50 mL of Luria-Bertani medium with the same antibiotics. After 3 h, 0.1 mM isopropylthio-β-galactoside was added, and the *E. coli* was further incubated in darkness at 28°C for 72 h. For the expression of *GmCCD7* or *GmCCD8*,

p3HA-GmCCD7 or p3HA-GmCCD8 was introduced into *E. coli* (BL21) containing a carotenoid-producing construct (pAC-zeaxanthin or pACCAR16ΔcrtX). The transformants were grown as described above and incubated for 24 h after adding isopropylthio-β-galactoside. Carotenoid cleavage activity was inferred from the absence of accumulating carotenoids (i.e. the absence of yellow color).

Cell pellets of *E. coli* cultures were resuspended in 80% acetone and concentrated. After redissolving in methanol, 10-μL samples were used for HPLC. Assays were performed in ambient conditions using a Prostar 230 ternary gradient pump, a Prostar 430 autosampler, and a Prostar 335 photodiode array detector (Varian). Separation was carried out on a 4.6 × 150-mm carotenoid column (YMC Co.) with a particle size of 3 μm. The mobile phase consisted of solvent A (methanol:tert-butyl methyl ether, 10:90, v/v) and solvent B (water:methanol, 5:95, v/v). A linear gradient was used (10% solvent A at 0 min, 65% solvent A at 40 to 45 min, 95% solvent A at 45 to 50 min). The flow rate was maintained at 1 mL min⁻¹, and the chromatographic profile was recorded at 470 nm. MS data for the carotenoids were obtained using the 1200L liquid chromatography/MS apparatus (Varian). MS conditions were as follows: Atmospheric Pressure Chemical Ionization positive ion mode; mass range, mass-to-charge ratio of 200 to 800; corona current, 2.0 μA; nebulizing gas pressure (nitrogen), 60 p.s.i.; drying gas (nitrogen) flow rate, 4 L min⁻¹; drying gas temperature, 300°C.

Subcellular Localization of GmBCHs Using Arabidopsis Protoplasts and EM Immunogold Labeling

To make GFP fusion constructs, the full-length cDNAs of the *GmBCHs* were amplified by PCR with *Pfu* DNA polymerase (Corebio) using primers (Supplemental Table S2) containing *XbaI* and *BamHI* sites and fused in frame to *GFP*. To make a truncated *GmBCH2-GFP*, a part of *GmBCH2* (corresponding to amino acids 48–314) was used. To make a fusion of *GmBCH1-GFP* with the transit peptide of *GmBCH2*, we used a region of *GmBCH2* corresponding to amino acids 1 to 47. Protoplasts isolated from Arabidopsis (*Arabidopsis thaliana*) were transfected by the polyethylene glycol method as described by Yoo et al. (2007). After 16 h of incubation, fluorescence was examined with a fluorescence microscope.

To make the transgenic plants expressing *GmBCH1-GFP*, *GmBCH2-GFP*, or *GmBCH3-GFP* for EM immunogold labeling, fusions of *GmBCHs-GFP* under the control of the CaMV 35S promoter were inserted between the *HindIII*/*EcoRI* sites of pCAMBIA3301. Transgenic nodules were produced according to Lee et al. (2005). Immunoelectron microscopic studies were performed according to Lin et al. (2011). Sections of 27-d-old nodule on copper grids were labeled with anti-GFP rabbit antibody (Abcam) and then with 10-nm gold-conjugated goat anti-rabbit antibody (Abcam). The sections were viewed in a JSM-1200EX II transmission electron microscope (JEOL).

Generation of Transgenic Root Nodules

To make *GmBCH(1+3)-RNAi* and *GmBCH2-RNAi* constructs, a 230 bp-fragment targeting both *GmBCH1* and *GmBCH3* and a 180 bp-fragment of *GmBCH2* were amplified by PCR with *Pfu* DNA polymerase (Corebio) using the primers shown in Supplemental Table S2. The amplified fragments were inserted into the *HindIII*/*XbaI* and *XhoI*/*KpnI* sites of pKANNIBAL (Wesley et al., 2001). The *GmBCH(1+3)-RNAi* construct was transferred into the binary plasmid pCAMBIA1304, and the resulting plasmid was introduced into *Agrobacterium rhizogenes* (K599) by the freeze-thaw method. Hairy roots emerging after infection with the agrobacteria were examined for *GUS* expression in order to identify the transgenic hairy roots, and only one transgenic hairy root in each plant was spared to be used for nodulation, removing all the others (Lee et al., 2005).

Acetylene Reduction Assay

Ethylenes produced per g (fresh weight) of nodules were determined as described previously (Oh et al., 2001).

Transmission Electron Microscopy

Nodule specimens (approximately 1 × 3 mm² with 1-mm-thick underlying tissues) from transgenic roots containing the *GmBCH(1+3)-RNAi* construct were excised with a razor blade and processed as reported previously (Kim,

2008). After metal staining, the sections were examined with a transmission electron microscope (JEM-1010; JEOL) operated at an accelerating voltage of 80 kV.

Supplemental Data

The following materials are available in the online version of this article.

Supplemental Figure S1. Comparison of the amino acid sequences of BCHs, ZEPs, VDEs, NCED1s, CCD7s, CCD8s, and CCD1s.

Supplemental Figure S2. The upstream region of *GmBCH1* isolated by DNA walking.

Supplemental Figure S3. Assessment of the PCR efficiency of primer sets for *GmBCHs*.

Supplemental Figure S4. Assessment of probes for in situ hybridization.

Supplemental Figure S5. Expression of *GmBCH2-GUS* and *GmBCH3-GUS* in transgenic soybean nodules measured by fluorometric assay of GUS.

Supplemental Figure S6. Subcellular localization of N-terminally deleted *GmBCH2* and a fusion of *GmBCH1* with the transit peptide of *GmBCH2*.

Supplemental Figure S7. DNA sequences used in preparing for *GmBCH1*+3)-RNAi and *GmBCH2*-RNAi constructs.

Supplemental Figure S8. Statistical analyses of nodule weight and gene expression in *GmBCH1*+3)-RNAi nodules.

Supplemental Figure S9. EM analysis of *GmBCH1*+3)-RNAi nodules.

Supplemental Figure S10. Expression of *GmZEP3* in soybean.

Supplemental Figure S11. Functional assay of *GmCCD7* and *GmCCD8* in β -carotene-accumulating *E. coli*.

Supplemental Table S1. RNA-Seq expression data for soybean genes in various tissues.

Supplemental Table S2. Primers used for gene cloning and gene expression by real-time RT-PCR.

ACKNOWLEDGMENTS

We thank Drs. Norihiko Misawa and Francis X. Cunningham, Jr., for generously providing pACCAR16 Δ actX and pAC-zeaxanthin, respectively.

Received January 26, 2013; accepted May 14, 2013; published May 22, 2013.

LITERATURE CITED

- Alder A, Holdermann I, Beyer P, Al-Babili S** (2008) Carotenoid oxygenases involved in plant branching catalyze a highly specific conserved apocarotenoid cleavage reaction. *Biochem J* **416**: 289–296
- Auldrige ME, Block A, Vogel JT, Dabney-Smith C, Mila I, Bouzayen M, Magallanes-Lundback M, DellaPenna D, McCarty DR, Klee HJ** (2006a) Characterization of three members of the Arabidopsis carotenoid cleavage dioxygenase family demonstrates the divergent roles of this multifunctional enzyme family. *Plant J* **45**: 982–993
- Auldrige ME, McCarty DR, Klee HJ** (2006b) Plant carotenoid cleavage oxygenases and their apocarotenoid products. *Curr Opin Plant Biol* **9**: 315–321
- Booker J, Auldrige M, Wills S, McCarty D, Klee H, Leyser O** (2004) MAX3/CCD7 is a carotenoid cleavage dioxygenase required for the synthesis of a novel plant signaling molecule. *Curr Biol* **14**: 1232–1238
- Bouvier F, Isner JC, Dogbo O, Camara B** (2005) Oxidative tailoring of carotenoids: a prospect towards novel functions in plants. *Trends Plant Sci* **10**: 187–194
- Bouvier F, Keller Y, d'Harlingue A, Camara B** (1998) Xanthophyll biosynthesis: molecular and functional characterization of carotenoid hydroxylases from pepper fruits (*Capsicum annuum* L.). *Biochim Biophys Acta* **1391**: 320–328
- Cazzonelli CI, Pogson BJ** (2010) Source to sink: regulation of carotenoid biosynthesis in plants. *Trends Plant Sci* **15**: 266–274
- Conover WJ** (1971) Practical Nonparametric Statistics. John Wiley & Sons, New York, pp 97–104
- Davison PA, Hunter CN, Horton P** (2002) Overexpression of β -carotene hydroxylase enhances stress tolerance in Arabidopsis. *Nature* **418**: 203–206
- DellaPenna D, Pogson BJ** (2006) Vitamin synthesis in plants: tocopherols and carotenoids. *Annu Rev Plant Biol* **57**: 711–738
- Ding Y, Kalo P, Yendrek C, Sun J, Liang Y, Marsh JF, Harris JM, Oldroyd GE** (2008) Abscisic acid coordinates nod factor and cytokinin signaling during the regulation of nodulation in *Medicago truncatula*. *Plant Cell* **20**: 2681–2695
- Floss DS, Schliemann W, Schmidt J, Strack D, Walter MH** (2008) RNA interference-mediated repression of *MtCCD1* in mycorrhizal roots of *Medicago truncatula* causes accumulation of C27 apocarotenoids, shedding light on the functional role of CCD1. *Plant Physiol* **148**: 1267–1282
- Galpaz N, Ronen G, Khalfa Z, Zamir D, Hirschberg J** (2006) A chromoplast-specific carotenoid biosynthesis pathway is revealed by cloning of the tomato white-flower locus. *Plant Cell* **18**: 1947–1960
- Giuliano G, Tavazza R, Diretto G, Beyer P, Taylor MA** (2008) Metabolic engineering of carotenoid biosynthesis in plants. *Trends Biotechnol* **26**: 139–145
- Gomez-Roldan V, Fervas S, Brewer PB, Puech-Pagès V, Dun EA, Pillot JP, Letisse F, Matusova R, Danoun S, Portais JC, et al** (2008) Strigolactone inhibition of shoot branching. *Nature* **455**: 189–194
- Grünewald K, Hirschberg J, Hagen C** (2001) Ketocarotenoid biosynthesis outside of plastids in the unicellular green alga *Haematococcus pluvialis*. *J Biol Chem* **276**: 6023–6029
- Ha SH, Liang YS, Jung H, Ahn MJ, Suh SC, Kweon SJ, Kim DH, Kim YM, Kim JK** (2010) Application of two bicistronic systems involving 2A and IRES sequences to the biosynthesis of carotenoids in rice endosperm. *Plant Biotechnol J* **8**: 928–938
- Jefferson RA, Kavanagh TA, Bevan MW** (1987) GUS fusions: beta-glucuronidase as a sensitive and versatile gene fusion marker in higher plants. *EMBO J* **6**: 3901–3907
- Kim J, Smith JJ, Tian L, Dellapenna D** (2009) The evolution and function of carotenoid hydroxylases in *Arabidopsis*. *Plant Cell Physiol* **50**: 463–479
- Kim KW** (2008) Visualization of micromorphology of leaf epicuticular waxes of the rubber tree *Ficus elastica* by electron microscopy. *Micron* **39**: 976–984
- Kistner C, Winzer T, Pitzschke A, Mulder L, Sato S, Kaneko T, Tabata S, Sandal N, Stougaard J, Webb KJ, et al** (2005) Seven *Lotus japonicus* genes required for transcriptional reprogramming of the root during fungal and bacterial symbiosis. *Plant Cell* **17**: 2217–2229
- Kopsell DA, Kopsell DE** (2006) Accumulation and bioavailability of dietary carotenoids in vegetable crops. *Trends Plant Sci* **11**: 499–507
- Lee MY, Shin KH, Kim YK, Suh JY, Gu YY, Kim MR, Hur YS, Son O, Kim JS, Song E, et al** (2005) Induction of thioredoxin is required for nodule development to reduce reactive oxygen species levels in soybean roots. *Plant Physiol* **139**: 1881–1889
- Libault M, Farmer A, Joshi T, Takahashi K, Langley RJ, Franklin LD, He J, Xu D, May G, Stacey G** (2010) An integrated transcriptome atlas of the crop model *Glycine max*, and its use in comparative analyses in plants. *Plant J* **63**: 86–99
- Lin WL, Dickson DW, Sahara N** (2011) Immunoelectron microscopic and biochemical studies of caspase-cleaved tau in a mouse model of tauopathy. *J Neuropathol Exp Neurol* **70**: 779–787
- Lu S, Li L** (2008) Carotenoid metabolism: biosynthesis, regulation, and beyond. *J Integr Plant Biol* **50**: 778–785
- Maritz JS** (1981) Distribution-Free Statistical Methods. Chapman & Hall, New York, p 217
- Misawa N, Nakagawa M, Kobayashi K, Yamano S, Izawa Y, Nakamura K, Harashima K** (1990) Elucidation of the *Erwinia uredovora* carotenoid biosynthetic pathway by functional analysis of gene products expressed in *Escherichia coli*. *J Bacteriol* **172**: 6704–6712
- Oh HS, Son O, Chun JY, Stacey G, Lee MS, Min KH, Song ES, Cheon CI** (2001) The *Bradyrhizobium japonicum* hsfA gene exhibits a unique developmental expression pattern in cowpea nodules. *Mol Plant Microbe Interact* **14**: 1286–1292
- Ohmiya A, Kishimoto S, Aida R, Yoshioka S, Sumitomo K** (2006) Carotenoid cleavage dioxygenase (CmCCD4a) contributes to white color formation in Chrysanthemum petals. *Plant Physiol* **142**: 1193–1201
- Oldroyd GE, Murray JD, Poole PS, Downie JA** (2011) The rules of engagement in the legume-rhizobial symbiosis. *Annu Rev Genet* **45**: 119–144

- Oldroyd GED, Harrison MJ, Paszkowski U (2009) Reprogramming plant cells for endosymbiosis. *Science* **324**: 753–754
- Ott T, van Dongen JT, Günther C, Krusell L, Desbrosses G, Vigeolas H, Bock V, Czechowski T, Geigenberger P, Udvardi MK (2005) Symbiotic leghemoglobins are crucial for nitrogen fixation in legume root nodules but not for general plant growth and development. *Curr Biol* **15**: 531–535
- Paine JA, Shipton CA, Chaggar S, Howells RM, Kennedy MJ, Vernon G, Wright SY, Hinchliffe E, Adams JL, Silverstone AL, et al (2005) Improving the nutritional value of Golden Rice through increased provitamin A content. *Nat Biotechnol* **23**: 482–487
- Rao AV, Rao LG (2007) Carotenoids and human health. *Pharmacol Res* **55**: 207–216
- Ruyter-Spira C, Al-Babili S, van der Krol S, Bouwmeester H (2013) The biology of strigolactones. *Trends Plant Sci* **18**: 72–83
- Schmutz J, Cannon S, Schlueter J, Ma J, Mitros T, Nelson W, Hyten D, Song Q, Thelen J, Cheng J, et al (2010) Genome sequence of the paleopolyploid soybean. *Nature* **463**: 178–183
- Schwartz SH, Qin X, Loewen MC (2004) The biochemical characterization of two carotenoid cleavage enzymes from *Arabidopsis* indicates that a carotenoid-derived compound inhibits lateral branching. *J Biol Chem* **279**: 46940–46945
- Severin AJ, Woody JL, Bolon Y-T, Joseph B, Diers BW, Farmer AD, Muehlbauer GJ, Nelson RT, Grant D, Specht JE, et al (2010) RNA-Seq Atlas of *Glycine max*: a guide to the soybean transcriptome. *BMC Plant Biol* **10**: 160
- Simkin AJ, Moreau H, Kuntz M, Pagny G, Lin C, Tanksley S, McCarthy J (2008) An investigation of carotenoid biosynthesis in *Coffea canephora* and *Coffea arabica*. *J Plant Physiol* **165**: 1087–1106
- Singh S, Parniske M (2012) Activation of calcium- and calmodulin-dependent protein kinase (CCaMK), the central regulator of plant root endosymbiosis. *Curr Opin Plant Biol* **15**: 444–453
- Snowden KC, Simkin AJ, Janssen BJ, Templeton KR, Loucas HM, Simons JL, Karunairetnam S, Gleave AP, Clark DG, Klee HJ (2005) The *Decreased apical dominance1/Petunia hybrida* CAROTENOID CLEAVAGE DIOXYGENASE8 gene affects branch production and plays a role in leaf senescence, root growth, and flower development. *Plant Cell* **17**: 746–759
- Stacey G, Libault M, Brechenmacher L, Wan J, May GD (2006) Genetics and functional genomics of legume nodulation. *Curr Opin Plant Biol* **9**: 110–121
- Strack D, Fester T (2006) Isoprenoid metabolism and plastid reorganization in arbuscular mycorrhizal roots. *New Phytol* **172**: 22–34
- Stracke S, Kistner C, Yoshida S, Mulder L, Sato S, Kaneko T, Tabata S, Sandal N, Stougaard J, Szczyglowski K, et al (2002) A plant receptor-like kinase required for both bacterial and fungal symbiosis. *Nature* **417**: 959–962
- Sun Z, Gantt E, Cunningham FX Jr (1996) Cloning and functional analysis of the β -carotene hydroxylase of *Arabidopsis thaliana*. *J Biol Chem* **271**: 24349–24352
- Suzuki A, Akune M, Kogiso M, Imagama Y, Osuki K, Uchiumi T, Higashi S, Han SY, Yoshida S, Asami T, et al (2004) Control of nodule number by the phytohormone abscisic acid in the roots of two leguminous species. *Plant Cell Physiol* **45**: 914–922
- Takaichi S, Mimuro M (1998) Distribution and geometric isomerism of neoxanthin in oxygenic phototrophs: 9'-*cis*, a sole molecular form. *Plant Cell Physiol* **39**: 968–977
- Tominaga A, Nagata M, Futsuki K, Abe H, Uchiumi T, Abe M, Kucho K, Hashiguchi M, Akashi R, Hirsch AM, et al (2009) Enhanced nodulation and nitrogen fixation in the abscisic acid low-sensitive mutant enhanced nitrogen fixation1 of *Lotus japonicus*. *Plant Physiol* **151**: 1965–1976
- Tsuchiya Y, McCourt P (2009) Strigolactones: a new hormone with a past. *Curr Opin Plant Biol* **12**: 556–561
- Ubuka T, Bentley GE (2009) Identification, localization, and regulation of passerine GnRH-I messenger RNA. *J Endocrinol* **201**: 81–87
- Umehara M, Hanada A, Yoshida S, Akiyama K, Arite T, Takeda-Kamiya N, Magome H, Kamiya Y, Shirasu K, Yoneyama K, et al (2008) Inhibition of shoot branching by new terpenoid plant hormones. *Nature* **455**: 195–200
- Vandesompele J, De Preter K, Pattyn F, Poppe B, Van Roy N, De Paepe A, Speleman F (2002) Accurate normalization of real-time quantitative RT-PCR data by geometric averaging of multiple internal control genes. *Genome Biol* **3**: RESEARCH0034
- Vogel JT, Walter MH, Giavalisco P, Lytovchenko A, Kohlen W, Charnikhova T, Simkin AJ, Goulet C, Strack D, Bouwmeester HJ, et al (2010) SICCD7 controls strigolactone biosynthesis, shoot branching and mycorrhiza-induced apocarotenoid formation in tomato. *Plant J* **61**: 300–311
- von Lintig J (2010) Colors with functions: elucidating the biochemical and molecular basis of carotenoid metabolism. *Annu Rev Nutr* **30**: 35–56
- Walter MH, Floss DS, Strack D (2010) Apocarotenoids: hormones, mycorrhizal metabolites and aroma volatiles. *Planta* **232**: 1–17
- Weigel D, Glazebrook J (2002) *Arabidopsis: A Laboratory Manual*. Cold Spring Harbor Laboratory Press, Cold Spring Harbor, NY, pp 212–214
- Wesley SV, Helliwell CA, Smith NA, Wang MB, Rouse DT, Liu Q, Gooding PS, Singh SP, Abbott D, Stoutjesdijk PA, et al (2001) Construct design for efficient, effective and high-throughput gene silencing in plants. *Plant J* **27**: 581–590
- Ye X, Al-Babili S, Klöti A, Zhang J, Lucca P, Beyer P, Potrykus I (2000) Engineering the provitamin A (β -carotene) biosynthetic pathway into (carotenoid-free) rice endosperm. *Science* **287**: 303–305
- Yoo SD, Cho YH, Sheen J (2007) *Arabidopsis* mesophyll protoplasts: a versatile cell system for transient gene expression analysis. *Nat Protoc* **2**: 1565–1572
- Yu B, Lydiate DJ, Schäfer UA, Hannoufa A (2007) Characterization of a beta-carotene hydroxylase of *Adonis aestivalis* and its expression in *Arabidopsis thaliana*. *Planta* **226**: 181–192